APL Materials

RESEARCH ARTICLE | AUGUST 14 2024

Spin magnetotransport in rare-earth iron garnet (REIG)/Pt: Effects of modulated bulk and REIG/Pt interfaces

Pei Gen Li ; Sheung Mei Ng ; Xin Yuan ; Fu Xiang Zhang ; Hon Fai Wong; Zhi Qin Chu ; Peng Cao ; Chi Wah Leung

APL Mater. 12, 081114 (2024)
https://doi.org/10.1063/5.0215071

Spin magnetotransport in rare-earth iron garnet (REIG)/Pt: Effects of modulated bulk and REIG/Pt interfaces

Cite as: APL Mater. 12, 081114 (2024); doi: 10.1063/5.0215071
Submitted: 22 April 2024 • Accepted: 30 July 2024 •
Published Online: 14 August 2024

Pei Gen Li,[1] Sheung Mei Ng,[1] Xin Yuan,[1,2] Fu Xiang Zhang,[2] Hon Fai Wong,[1] Zhi Qin Chu,[3] Peng Cao,[4] and Chi Wah Leung[1,a)]

AFFILIATIONS

[1] Department of Applied Physics, The Hong Kong Polytechnic University, Hong Kong, China
[2] Songshan Lake Materials Laboratory, Dongguan, Guangdong 523808, China
[3] Department of Electrical and Electronic Engineering, The University of Hong Kong, Pokfulam Road, Hong Kong, China
[4] Department of Diagnostic Radiology, The University of Hong Kong, Pokfulam Road, Hong Kong, China

[a)] **Author to whom correspondence should be addressed:** dennis.leung@polyu.edu.hk

ABSTRACT

The intrinsic magnetization compensation behaviors of rare-earth iron garnets (REIGs) make the material promising for applications in ultrafast spin storage devices. REIG/heavy metal heterostructures such as TbIG/Pt often display two sign crossovers of anomalous Hall effect resistance with varying temperatures. One of these crossovers is attributed to the magnetization compensation of REIG, and the other to the competition between the magnetic proximity effect and the spin Hall effect. Here, we design trilayer REIG heterostructures based on two rare-earth species (Tb and Eu). We modulate the layer stacking of the TbIG/EuIG/TbIG sandwich with a fixed total thickness and explore the contributions of REIG bulk and REIG/Pt interfaces on these two crossover points. As TbIG gradually moves away from Pt, the compensation temperature shows some fluctuations. However, when TbIG is entirely out of contact with Pt, the second crossover point undergoes a change that shows REIG/Pt interface dependency. The results highlight the dominance of REIG bulk on the compensation behavior and the interface sensitivity of the second crossover point. This study provides a reference for designing controllable spintronics devices, such as magnon valve applications.

I. INTRODUCTION

Rare-earth iron garnets (REIGs) with magnetization compensation have been widely studied recently. Magnetization compensation in REIG refers to the condition at which the net magnetization temporarily vanishes due to the different temperature dependences between antiparallel-aligned moments of RE and Fe ions.[1–5] Examples of compensated REIG include $Tb_3Fe_5O_{12}$ (TbIG),[6] $Dy_3Fe_5O_{12}$ (DyIG),[7,8] and $Gd_3Fe_5O_{12}$ (GdIG).[9,10] Researchers have extensively investigated the compensation behavior, especially in REIG/Pt systems, through methods such as the spin Seebeck effect (SSE),[11,12] anomalous Hall effect (AHE),[13,14] and spin Hall effect (SHE),[15,16] showing the tremendous potential application of ferrimagnets in fields such as ultrafast magnetization switching.

Compensation behavior in REIG thin films exhibits tunability under varying deposition conditions or substrates. Li *et al.* deposited single layer TbIG on different substrates, causing changes in the strain of the films and realizing compensation temperature (T_{comp}) adjustment from 196 K (GGG substrates) to 160 K (GSGG substrates).[17] Similarly, adjusting T_{comp} through strain modulation was achieved by changing the thickness of the REIG films.[6] T_{comp} can also be varied by adjusting the atomic ratio of RE ions in REIG.[18,19] These efforts demonstrate the diverse strategies available for regulating magnetization compensation behavior, providing an experimental and theoretical basis for designing more complex systems.

Recently, REIG heterojunctions were studied in combination with heavy metals (HM). In some of such systems, the

temperature-dependent anomalous Hall effect resistance (R_{AHE}) exhibits two sign-flipping events. The first flipping originates from the competition for antiparallel alignment between the RE and Fe moments, which corresponds to the T_{comp} of the material. The other sign flipping event (sometimes referred to as the T_1 point) differs from T_{comp} in that it has a strong correlation with the REIG/HM interface. This crossover is typically attributed to the competition between the spin Hall effect and the magnetic proximity effect (MPE)[13,20] and has been observed in systems such as GdIG/Pt and TbIG/Pt.[3,21] For example, TbIG/Pt shows the first sign reversal at T_{comp} (about 220 K), which is accompanied by a divergence of coercivity and an abrupt change in the R_{AHE} sign. The second sign crossover point is observed below $T_{comp,}$ and the sign change takes place more gradually.[22]

The quality of the REIG/Pt interface plays a vital role in spin Hall magnetotransport. For example, the dusting of Cu at the TmIG/Pt interface was used to examine the relative contributions of the spin Hall effect and magnetic proximity effect.[23] Meanwhile, the impact on T_{comp} through a fixed REIG/HM interface but with modulated composition in the REIG film bulk is seldom reported. In addition, the influence of different REIG/HM interfaces (or additional interfaces generated by stacking multiple REIG layers) on the sign reversal behavior may not be easily assessable. The roles of the modulated REIG bulk as well as the REIG/Pt interface on the spin magnetotransport in the REIG/Pt system are worth exploring.

In this work, we modulate the REIG bulk by inserting a different iron garnet of fixed thickness at different locations along the film growth direction. To achieve this goal, two different garnets (1-REIG and 2-REIG) with similar lattice constants that demonstrate perpendicular magnetic anisotropy (PMA) are desired, as they facilitate epitaxial film growth and allow magnetotransport measurement in the PMA state. In addition, by choosing the REIG combinations such that only one of them exhibits magnetization compensation, the occurrence of multiple T_{comp} can be avoided.

When designing the REIG sandwich, a 2-REIG layer of fixed thickness is gradually moved from the bottom of the stack (i.e., in direct contact with the substrate) to the top surface. The deposition sequence, therefore, changes from substrate/2-REIG/1-REIG through the sandwich structure of substrate/1-REIG/2-REIG/1-REIG and finally becomes substrate/1-REIG/2-REIG; the total thickness of 1-REIG in all samples is kept constant. This system allows the exploration of the impact of 2-REIG as it progressively approaches the top surface, which eventually will be in direct contact with Pt. Unlike single-layer or bilayer REIG systems with varying thicknesses, the overall magnetization of such a sandwich structure is kept constant, given identical 2-REIG and aggregated 1-REIG thicknesses in the samples. This eliminates the possible complications due to the variation in total magnetization of the REIG heterostructure.

Here, we choose TbIG (1-REIG) and EuIG (2-REIG) on the GGG (111) substrate as our system of investigation. The similar lattice constants of TbIG (12.436 Å)[24] and EuIG (12.500 Å)[25] permit epitaxial growth on GGG (12.376 Å)[25] with PMA behavior in (111) orientation.[26] Furthermore, EuIG does not possess compensation behavior,[27] facilitating the observation of T_{comp} of TbIG through R_{AHE}–H measurements across a Pt Hall bar deposited on top of the REIG stack. Temperature dependent R_{AHE} measurements will probe the impact of the location of the EuIG layer in the TbIG/EuIG/TbIG stack and the presence of additional EuIG/TbIG interfaces.

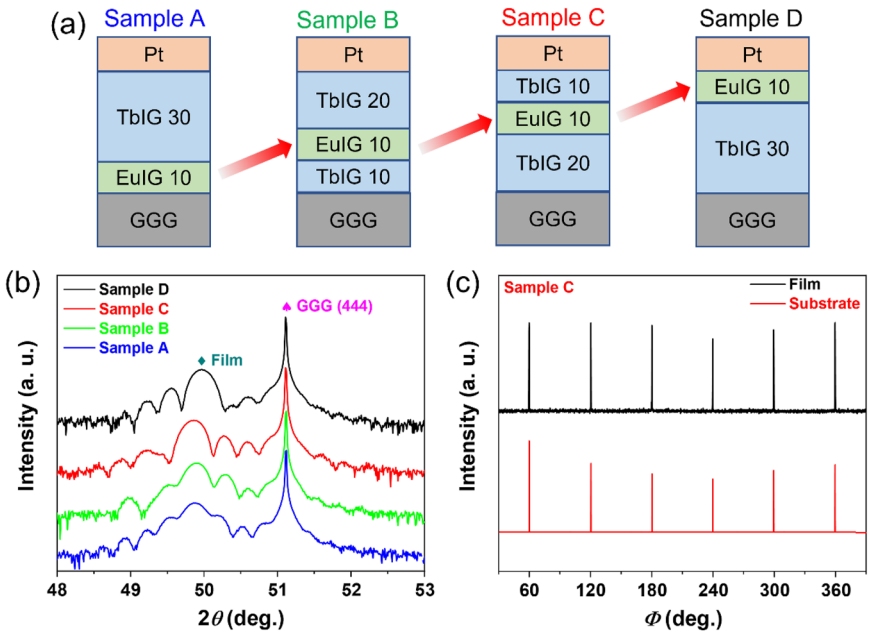

FIG. 1. (a) Schematic illustration of sandwich structure device (samples A to D). Numbers refer to the thickness of different REIG layers in nm. (b) XRD 2θ scan profiles of the samples. (c) XRD φ scan of sample C, showing six-fold symmetry and epitaxial relations between the multilayer and GGG substrate.

II. EXPERIMENTAL DETAILS

As shown in Fig. 1(a), four different stacks of GGG (111)/TbIG (x nm)/EuIG (10 nm)/TbIG (30-x nm) films are deposited using pulsed laser deposition (PLD), which are then covered with a Pt layer with Hall-bar geometry. Among the set of samples, the EuIG (10 nm) is gradually moved away from the substrate (sample A) and eventually comes into direct contact with Pt (sample D). A sandwich structure will be formed, among which samples A–C have the same TbIG/Pt interface while sample D has a EuIG/Pt interface. The total TbIG and EuIG thicknesses are kept at 40 nm in all samples. The deposition parameters and Hall device fabrication procedures shown in previous work are used in this paper.[22]

The crystallinity of the samples was examined by high-resolution x-ray diffractometry (XRD). Spherical aberration-corrected transmission electron microscopy (TEM) was used to observe the distribution of elements and microstructure along the $[11\bar{2}]$ direction with an operating voltage of 300 kV and a collection angle of 25 mrad. TEM samples were prepared by focused ion beam microscopy (FIB). The thickness of the films was confirmed by high-resolution transmission electron microscopy (HR-TEM). Temperature-dependent hysteresis loops were measured by vibrating sample magnetometry (VSM) at room temperature. A physical property measurement system (PPMS) was used to measure the temperature-dependent R_{AHE} under an out-of-plane external field.

III. RESULTS AND DISCUSSIONS

Due to the slight difference in lattice constants among GGG (12.376 Å), TbIG (12.436 Å), and EuIG (12.500 Å),[24,25] the REIG layers are under in-plane compressive strain during their growth, as reflected through the shift of the film peaks in the XRD 2θ scans. As shown in Fig. 1(b), the 2θ peaks of films shift from 48.86° to 49.96° as the topmost TbIG completely exchanges with EuIG in the deposition sequence (samples A and D). Sample C does not seem to follow the continuous shift. The complexity of the additional TbIG/EuIG interfaces during the trilayer film deposition process could result in additional defects and complex stress.

The lattice mismatch η between the film material and substrate can be calculated as $\eta = |\frac{A_{sub}-B_{REIG}}{B_{REIG}}|$,[28] where A_{sub} is the lattice constant of substrates and B_{REIG} represents that of REIG bulk value. The calculated mismatch is $\eta_{GGG/TbIG} = 0.48\%$ and $\eta_{GGG/EuIG} = 0.99\%$, indicating the possible difference in stress states when exchanging the positions of two REIGs. An out-of-plane lattice spacing

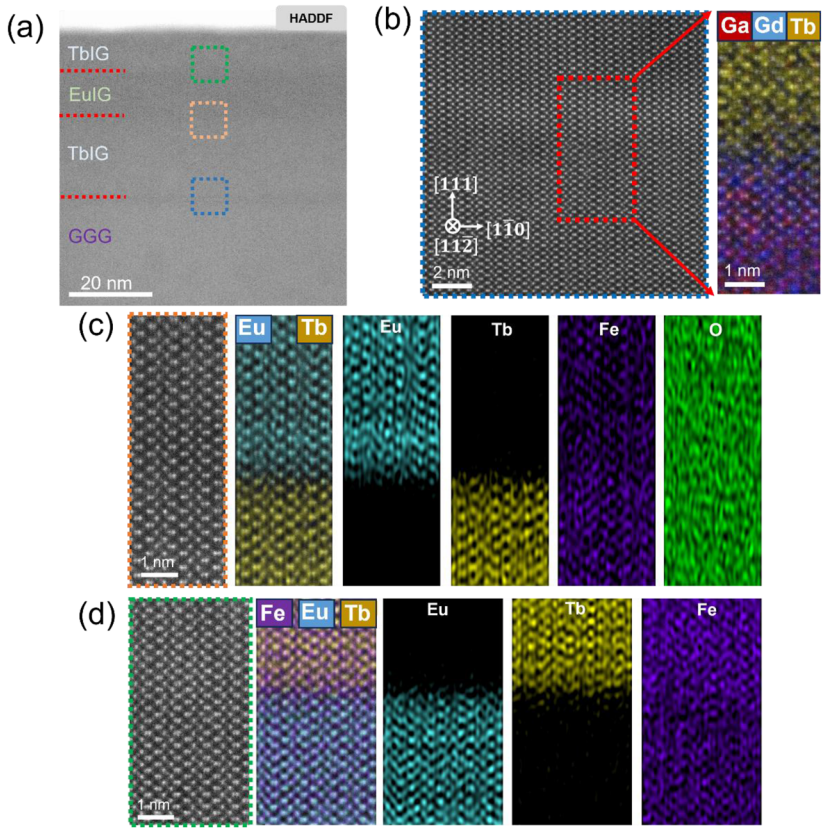

FIG. 2. (a) HAADF image of sample C, showing various interfaces (red dashed lines as guides to the eye). (b) Magnified GGG/TbIG interface extracted from the blue square of the HAADF image. A mixed Ga, Gd, and Tb element distribution (as revealed by EDS mapping) was extracted from the red region at the GGG/TbIG interface. The EDS mapping analysis of the TbIG/EuIG interface and the EuIG/TbIG interface, as extracted from the yellow and green regions in (a), is shown in (c) and (d), respectively.

d_{444} = 1.828 is extracted for sample A, which is slightly larger than that of sample D (d_{444} = 1.823 Å). It is likely that the TbIG layer plays a stress buffering role.[29] In addition, both REIGs show in-plane compressive strain, allowing the PMA behavior to be maintained in both REIGs on the GGG (111) substrate. The Laue oscillations of the sandwich film peaks also confirm the high crystallinity of the samples. The six-fold symmetry as shown by the φ scan of GGG and TbIG/EuIG/TbIG (642) peaks [Fig. 1(c)] indicates the epitaxial growth of the films.

To further analyze the epitaxy and interfacial element distribution, Fig. 2 shows the cross-sectional high-angle annular dark-field (HAADF) images of sample C along the [11$\bar{2}$] direction, accompanied by the energy-dispersive x-ray spectroscopy (EDS) images of GGG/TbIG, TbIG/EuIG, and EuIG/TbIG interfaces. In Fig. 2(a), from the substrate to the topmost TbIG film, the interfaces among REIG layers and with the GGG substrate can be identified by the red dashed lines in Fig. 2(a) and EDS mappings in Figs. 2(b)–2(d). The measured thickness of each REIG layer agrees well with the estimated deposition rate of our initial calibration sample. In addition, XRR was used to estimate the overall thickness of films in the series of samples for reference (Fig. S1 and Table S1 of the supplementary material). The results indicate that the thickness of all samples met expectations.

Elemental distribution analysis was conducted in regions from the three interfaces of sample C [blue, yellow, and green boxes in Fig. 2(a)]. For the substrate/TbIG interface [Fig. 2(b)], the minute lattice mismatch allows high-quality epitaxy and crystalline growth of the TbIG layer. It is noted that Gd (blue) and Tb (yellow) diffuse into each other's lattice positions, and the thickness of the transient layer is estimated at 1–2 nm. Such interdiffusion is common in REIG growth.[10,30,31] Considering the thickness of the transient layer is much smaller than the total thickness of the thin film, the influence of the transient layer on T_{comp} variations should be consistent in all samples. The uniform arrangement of the atomic structure indicates no obvious dislocations and vacancies, and the garnet structure is unchanged. Similarly, both TbIG/EuIG and EuIG/TbIG interfaces in Figs. 2(b) and 2(c) exhibit Tb/Eu interdiffusion and regular REIG atomic-scale structure, indicating good crystallinity of the layers. The results are consistent with the XRD 2θ and φ scan analyses in Fig. 1.

Unlike previous studies, which relied on modulating the TbIG layer thickness to regulate T_{comp} and interfacial spin magnetotransport,[6] in this work the aggregated thicknesses of EuIG (10 nm) and TbIG (30 nm) layers are fixed, with the separation between EuIG and Pt gradually varied from 30 nm to direct contact (i.e., EuIG moving from the bottom to the top of the stack). The design of such a sandwich TbIG/EuIG/TbIG structure helps to observe the impact of internal variation in REIG bulk on the spin magnetotransport. There are two factors worth noting, namely, the change of the REIG/Pt interface from TbIG/Pt to EuIG/Pt and the additional TbIG/EuIG interfaces in the sandwich structure.

Temperature-dependent anomalous Hall hysteresis loops were measured through processed Hall bar devices. R_{AHE}–H loops of all samples can be found in the supplementary material [Figs. S2–S5]. The coercivity (H_c) as measured at zero Hall resistance and anomalous Hall resistance at zero fields (R^0_{AHE}) were extracted from the temperature-dependent R_{AHE}–H curves [Figs. 3(a) and 3(b)]. Divergent H_c can be observed in all samples in Fig. 3(a), indicating the existence of T_{comp}.[2,32,33] Because the antiparallel-aligned Tb^{3+} and Fe^{3+} moments in TbIG have different temperature dependences, the overall magnetization temporarily cancels out as temperature goes down, as reflected through the H_c divergence at T_{comp}.

Meanwhile, R^0_{AHE} that is related to spin transport at the REIG/Pt interface undergoes sign flipping near T_{comp}. As shown in Figs. 3(a) and 3(b), the R^0_{AHE} reversal and divergent H_c behavior occur essentially at the same temperatures. Considering the antiparallel coupling between Tb^{3+} and Fe^{3+}, R_{AHE} sign orientation is predominantly determined by Fe moment direction.[22] As the temperature goes down and passes through T_{comp}, the reoriented Fe^{3+} moment

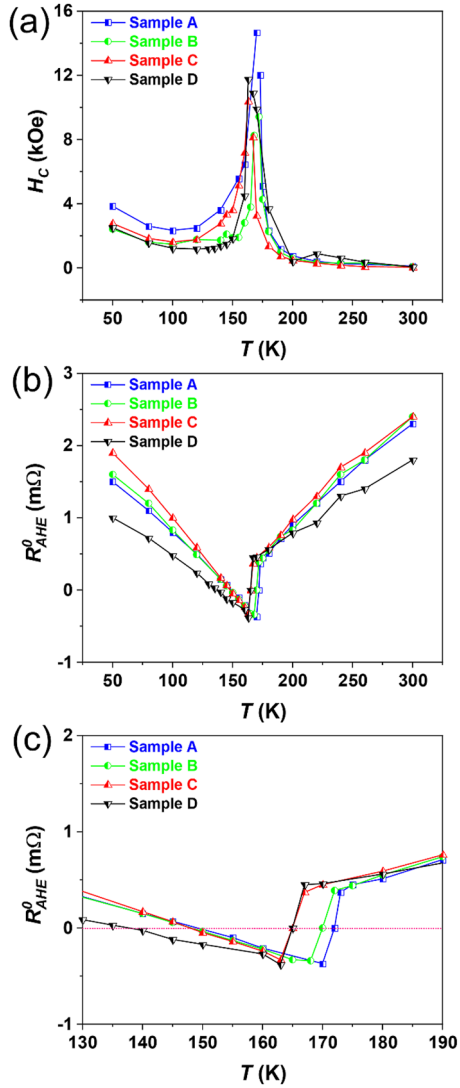

FIG. 3. Temperature-dependent H_c (a) and R^0_{AHE} (b) in GGG/TbIG/EuIG/TbIG samples. H_c and R^0_{AHE} are extracted from the R_{AHE}–H loops. (c) R^0_{AHE}–T curve in the region around the two crossover points.

results in the abrupt R^0_{AHE} sign reversal. Both R^0_{AHE} and H_c reflect the change of T_{comp} for these samples.

It is noticed that the R^0_{AHE}–T curves go through two sign reversals, which can be observed in Fig. 3(c). The first sign of reversal at higher temperatures takes place around T_{comp}. Notice that as TbIG gradually moves away from Pt, T_{comp} shows a fluctuation from 172 K (blue curve) to 165 K (black curve). In any case, the T_{comp} as measured from our TbIG/EuIG/TbIG sandwich samples is far from the bulk value of TbIG (248 K).[32] There are some possible reasons. For one, T_{comp} of TbIG in the thin film state has strong strain dependence. The epitaxial growth of REIG on the substrates results in strained growth, thereby altering the mutual coupling of internal atoms in REIGs.[17]

Meanwhile, the robust coupling between EuIG and TbIG is also a possible reason for the sharp decrease in T_{comp}. In TbIG, its overall magnetization is determined by Fe^{3+} above T_{comp}. With decreasing temperatures, the Tb^{3+} moment gradually dominates over Fe in the TbIG layer. In EuIG, although Eu^{3+} and Fe^{3+} show antiparallel alignment, Eu^{3+} does not contribute to the overall magnetization because of its zero angular momentum J at the ground state.[27,34] There is no magnetization compensation behavior in EuIG, and magnetic moment orientation is entirely decided by Fe^{3+}. However, in the sandwich structure, the Fe^{3+} ions in EuIG and TbIG are strongly ferromagnetically coupled, and the Tb^{3+} moment (in the TbIG) needs to compete with more Fe^{3+} moments (due to the presence of EuIG). Based on our previous work, we know that the T_{comp} of single-layer TbIG (30 nm) is around 220 K,[22] but it is dramatically changed in the sandwich structure (~170 K). A similar situation is observed in the in-plane YIG/GdIG system.[35]

It is noted that the T_{comp} between the four sandwich structural samples in this work also shows some fluctuations. With a fixed thickness of 40 nm among all our samples, we believe that the impact of stacking order on T_{comp} can be ignored, as T_{comp} is only related to the competition between RE and Fe moments throughout whole stack films. In other words, the nature of coupling at the TbIG/EuIG interface bears no relation to the appearance of T_{comp}, at least at the temperature ranges where our T_{comp} is observed. The R^0_{AHE}–T plots in Figs. 3(b) and 3(c) show no obvious trend in the fluctuations of T_{comp}. For example, the bilayer sample D and the sandwich sample C exhibit the same T_{comp}, while the T_{comp} of sandwich samples B and C is different. This indicates that the stacking order is not a decisive factor in the fluctuations of T_{comp}.

The ratio of TbIG thickness to the total film thickness ($t_{\mathrm{TbIG}}/t_{\mathrm{Total}}$) provides us with a more intuitive observation of T_{comp} fluctuations (Fig. S6 of the supplementary material). The slightly different $t_{\mathrm{TbIG}}/t_{\mathrm{Total}}$ ratio among the four samples, due to the run-to-run variations of deposited layer thickness, appears to justify the random fluctuations in T_{comp}. It should be noted that the RE:Fe ratio can also influence T_{comp}. Indeed, T_{comp} should increase with excessive RE and decrease due to the increase in Fe.[32,36] To this end, we analyzed the EDS data of sample C and extracted the RE:Fe ratio (Fig. S7 of the supplementary material). The measured RE:Fe ratio of 0.545 is lower than the expected value of 0.6 in the stoichiometric REIG structure. We cannot rule out run-to-run variations of the RE:Fe ratio that lead to the minute T_{comp} fluctuations observed across samples.

A second sign flipping T_1 can also be observed in Fig. 3(c), which occurs below T_{comp} with a more gradual R^0_{AHE} sign crossover. The T_1 point has been attributed to the competition between the MPE and the SHE.[37] A magnetic moment is induced in the Pt layer because of the MPE at the REIG/HM interface. This results in finite magnetic ordering in the Pt layer, hence the observation of AHE. Meanwhile, SHE is activated because the spin current transports across the REIG/HM interface and generates partial AHE, which competes with the MPE-induced AHE signal. This competition leads to the occurrence of the second R^0_{AHE} sign flip.

Interestingly, as shown in Fig. 3(c), when the REIG/HM interface is TbIG/Pt, T_1 remains the same at about 149 K (samples A–C), but it drops to 137 K as the interface changes to EuIG/Pt (sample D). The cause of T_1 variation is expected to be different from the T_{comp} modulation: T_{comp} is highly correlated with the moment competition of different sublattices, while T_1 point is related to the quality and magnetotransport of the REIG/HM interface. For the REIG/Pt system, the interface exchange coupling effect is dominated by Fe sublattices in the entire temperature range examined, since the d orbital of Fe has stronger delocalization behavior than the f orbital of RE.[37] Although the ground state of Eu^{3+} is $J = 0$, Eu^{3+} shows paramagnetic signals because of the second-order Zeeman effect.[34] Therefore, the magnetic contribution of Eu^{3+} cannot be ignored when studying interface sensitivity.

For an intuitive understanding of T_1 variation, a simple interface coupling model is presented in Fig. 4. Fe/Pt exchange coupling energy $J_{\mathrm{Fe/Pt}}$ dominates the interface coupling throughout the entire temperature range.[37] Meanwhile, Tb^{3+} and Eu^{3+} still have a small contribution. The different lattice constants between TbIG and EuIG would result in variations of RE–Pt and Fe–Pt bond lengths (and hence bond strengths), leading to a difference in MPE between the TbIG/Pt and EuIG/Pt interfaces.[38]

The difference in the contributions of total exchange coupling energy by Tb/Pt and Eu/Pt can be reflected by the slope of R^0_{AHE} throughout the entire temperature range. As shown in Fig. 3(b), the slopes of R^0_{AHE} of sample A–C with the TbIG/Pt interface appear to

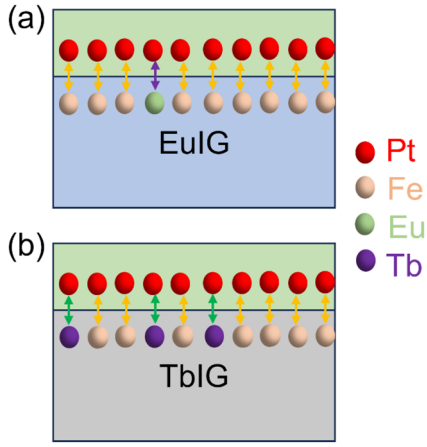

FIG. 4. Schematic of exchange coupling in the (a) EuIG/Pt and (b) TbIG/Pt interfaces. The number of colored balls represents the strength of the exchange coupling.

be steeper than that of sample D with the EuIG/Pt interface. Due to the total exchange energy of the interface, $J_{REIG/Pt}$ is in competition with $J_{Fe/Pt}$ and $J_{RE/Pt}$. Obviously, the difference in $J_{RE/Pt}$ will lead to variations in the $J_{REIG/Pt}$. The steeper slopes of R^0_{AHE} imply a more intense competition between $J_{Tb/Pt}$ and $J_{Fe/Pt}$. Thus, the exchange coupling energy of $J_{Tb/Pt}$ is considered stronger than that of $J_{Eu/Pt}$. In addition, both MPE and SHE are strongly related to $J_{REIG/Pt}$, but the AHE induced by MPE and SHE are opposite in sign.[13,38] Since the competition between MPE-induced and SHE induced-AHE leads to the occurrence of T_1, the variations of T_1 highlight the sensitivity of $J_{REIG/Pt}$ toward the RE species at the interface.

The roughness of the REIG/Pt interface is also a potential influencing factor for T_1 variation. In fact, AFM measurements (Fig. S8 of the supplementary material) for all samples with TbIG/Pt interfaces (samples A to C) suggest similar roughness (root-mean-squared values of 0.305, 0.371, and 0.382 nm, respectively). However, the roughness of sample D (0.537 nm), which possesses a EuIG/Pt interface, is higher than that of samples A–C with a TbIG/Pt interface. Previous work reported that the spin current transport would be affected by the interface roughness spin scattering,[39] which suggests its potential contribution to T_1 variations. Further investigations would be needed to identify the linkage between REIG/Pt interface quality and interfacial spin transport.

The impact of additional TbIG/EuIG interfaces on the two crossover points is also considered. The sandwich structure, as compared with bilayers, has an additional interface between EuIG and TbIG. To verify that PMA is retained in the sandwich REIG films, M–H loops were measured for all samples at room temperature with an out-of-plane applied field. The square loops (Fig. S9 of the supplementary material) indicate that all samples maintain PMA, due to in-plane compressive strain and a positive magnetostriction coefficient.[26,40]

The M–H loops in Fig. S9 also exhibit exchange bias behavior, as evidenced by the asymmetry about the zero field. Similar bias behavior can also be observed in the R_{AHE}–H loops (cf. Figs. S2 and S3 of the supplementary material). The exchange bias has been attributed to the antiferromagnetic coupling caused by the transient layer between the GGG substrate and the garnet films.[41] Our previous studies in a similar system of TbIG/YIG also suggest antiferromagnetic coupling at the interface of two garnets.[42] The exchange bias fields (H_{ex}) extracted from Fig. S9 (71, 87, 80, and 79 Oe for samples A to D) do not show obvious stacking sequence dependence, which suggests an independence of the number of TbIG/EuIG interfaces. It is, therefore, likely that the bias originates from the substrate/REIG interface.

Finally, the two crossover points of all samples are extracted for comparison in Fig. 5(b). All the samples show both T_{comp} and T_1. It can be noticed that the T_{comp} of four samples maintains ~170 K, even with the presence of additional TbIG/EuIG interfaces in the sandwich-type samples (samples B and C). The similar lattice constants of TbIG and EuIG result in good epitaxy and integrity of the atomic structure at the TbIG/EuIG interface, which is confirmed by the HAADF image in Fig. 2. This ensures minimal lattice distortion and magnetic moment loss for different sublattices. Combining the results of M_s and T_{comp}, as they are related to the net magnetic moment, we believe that the additional interface does not affect the magnetization compensation behavior under the same total thickness.

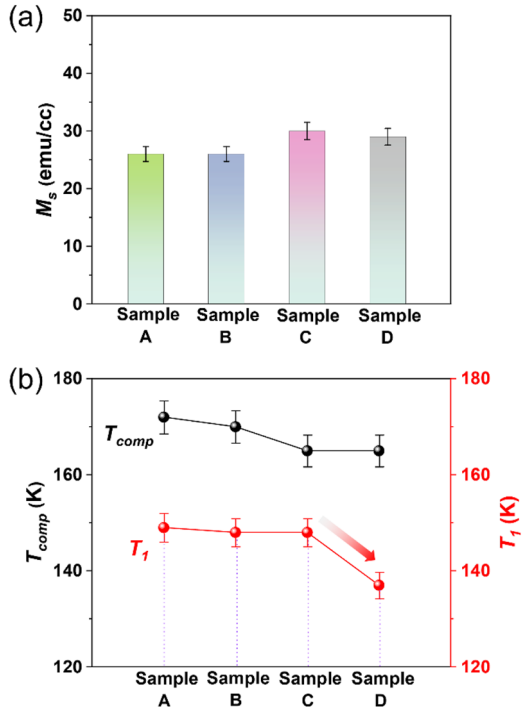

FIG. 5. (a) Comparison of saturation magnetization of all samples with the same thickness. (b) Comparison of T_{comp} and T_1 for all samples.

The fluctuations in M_s and T_{comp} of the TbIG/EuIG/TbIG samples can be attributed to the slight imbalance in stoichiometry caused by the transient layer. The formation of transient layers is a common phenomenon for the growth of multilayer thin films,[41,43] but the transient layer in our sandwich system retains a garnet structure (Fig. 2). The position of RE atoms can be occupied by either Tb or Eu in the transient layer, resulting in the fluctuations of M_s and T_{comp}. However, the thin transition layer (about 1–2 nm) can be ignored compared to the total thickness of the sandwich films (40 nm). Meanwhile, we cannot rule out the thickness variation among layers in the sandwich structure during the PLD growth, which can result in M_s and T_{comp} inconsistency.

As shown in Fig. 5(b), except for sample D (GGG/TbIG/EuIG/Pt), the other three samples maintain essentially the same T_1 (~149 K), indicating that the additional TbIG/EuIG interface does not affect the expression of T_1. As previously mentioned, the T_1 point has strong REIG/Pt interface sensitivity and is unrelated to the film's interior. This REIG/Pt interface sensitivity can be concluded by comparing the T_1 of sample D (GGG/TbIG/EuIG/Pt, 137 K) and sample A (GGG/EuIG/TbIG/Pt, 149 K). The interface exchange coupling energy between TbIG/Pt and EuIG/Pt is different, and there are also differences in the quality of the REIG/Pt interface, which contribute to the T_1 discrepancies. However, the specific TbIG/EuIG interface situation needs to be further discussed through thickness-dependent magnetization detection (e.g., by polarized neutron reflectometry) in the future.[30]

IV. CONCLUSION

In summary, the relative contributions of modulated REIG bulk and REIG/Pt interfaces on the spin Hall magnetotransport were studied in the TbIG/EuIG/TbIG/Pt system. We varied the layer stacking sequences of TbIG/EuIG/TbIG bulk while fixing the total thickness of the films. R_{AHE}–T plots indicate two events of R_{AHE} sign reversal, one at T_{comp} being related to the magnetization compensation behavior of the TbIG/EuIG/TbIG, and the other at T_1 arising from the competition of MPE and SHE at the REIG/Pt interface. The results indicate that T_{comp} changes need to consider the contribution of the whole REIG stack, and the stacking order hardly affects the expression of the compensation behavior of TbIG. In addition, the T_1 point exhibits strong REIG/Pt interface sensitivity. Different stacking orders can alter the interface quality, including interface exchange coupling energy and roughness, thereby affecting spin transport.

SUPPLEMENTARY MATERIAL

The supplementary material contains XRR, AFM, temperature-dependent R_{AHE} measurements, and M–H loops at room temperature for all samples. It also includes the EDS analysis of sample C.

ACKNOWLEDGMENTS

This work was supported by the Hong Kong Research Grants Council (Grant No. 15302320) and the Hong Kong Polytechnic University (ZVWC, CD6U). Support by the HKSAR Innovation and Technology Fund (ITF) through the Mainland-Hong Kong Joint Funding Scheme (MHKJFS, Grant No. MHP/070/20) is also acknowledged.

AUTHOR DECLARATIONS

Conflict of Interest

The authors have no conflicts to disclose.

Author Contributions

Pei Gen Li: Conceptualization (supporting); Data curation (lead); Formal analysis (lead); Investigation (lead); Methodology (lead); Writing – original draft (lead). **Sheung Mei Ng**: Investigation (supporting); Methodology (supporting); Writing – review & editing (equal). **Xin Yuan**: Investigation (supporting); Methodology (supporting); Writing – review & editing (equal). **Fu Xiang Zhang**: Investigation (supporting); Methodology (supporting); Writing – review & editing (supporting). **Hon Fai Wong**: Investigation (supporting); Methodology (supporting); Writing – review & editing (supporting). **Zhi Qin Chu**: Investigation (supporting); Methodology (supporting); Writing – review & editing (supporting). **Peng Cao**: Investigation (supporting); Methodology (supporting); Writing – review & editing (supporting). **Chi Wah Leung**: Conceptualization (lead); Formal analysis (lead); Funding acquisition (lead); Project administration (lead); Resources (lead); Supervision (lead); Writing – review & editing (equal).

DATA AVAILABILITY

The data that support the findings of this study are available from the corresponding author upon reasonable request.

REFERENCES

[1] S. Geprags, A. Kehlberger, F. D. Coletta, Z. Qiu, E. J. Guo, T. Schulz, C. Mix, S. Meyer, A. Kamra, M. Althammer, H. Huebl, G. Jakob, Y. Ohnuma, H. Adachi, J. Barker, S. Maekawa, G. E. W. Bauer, E. Saitoh, R. Gross, S. T. B. Goennenwein, and M. Klaui, Nat. Commun. **7**, 10452 (2016).
[2] M. V. Logunov, S. S. Safonov, A. S. Fedorov, A. A. Danilova, N. V. Moiseev, A. R. Safin, S. A. Nikitov, and A. Kirilyuk, Phys. Rev. Appl. **15**, 064024 (2021).
[3] Y. K. Liu, H. F. Wong, K. K. Lam, K. H. Chan, C. L. Mak, and C. W. Leung, J. Magn. Magn. Mater. **468**, 235 (2018).
[4] B. W. Dong, J. Cramer, K. Ganzhorn, H. Y. Yuan, E. J. Guo, S. T. B. Goennenwein, and M. Klaui, J. Phys. Condens. Matter. **30**, 035802 (2018).
[5] Y. J. Hong, J. S. Kum, I. B. Shim, and C. S. Kim, IEEE Trans. Magn. **40**, 2808 (2004).
[6] J. M. Liang, X. W. Zhao, Y. K. Liu, P. G. Li, S. M. Ng, H. F. Wong, W. F. Cheng, Y. Zhou, J. Y. Dai, C. L. Mak, and C. W. Leung, Appl. Phys. Lett. **122**, 242401 (2023).
[7] J. J. Bauer, P. Quarterman, A. J. Grutter, B. Khurana, S. Kundu, K. A. Mkhoyan, J. A. Borchers, and C. A. Ross, Phys. Rev. B **104**, 094403 (2021).
[8] J. J. Bauer, E. R. Rosenberg, S. Kundu, K. A. Mkhoyan, P. Quarterman, A. J. Grutter, B. J. Kirby, J. A. Borchers, and C. A. Ross, Adv. Electron. Mater. **6**, 1900820 (2020).
[9] Y. Li, D. Zheng, C. Liu, C. Zhang, B. Fang, A. Chen, Y. Ma, A. Manchon, and X. Zhang, ACS Nano **16**, 8181 (2022).
[10] L. Liu, Z. Fan, Z. Chen, Z. Chen, Z. Ye, H. Zheng, Q. Zeng, W. Jia, S. Li, N. Wang, J. Liu, L. Ma, T. Lin, M. Qiu, S. Li, P. Han, J. Shi, and H. An, Appl. Phys. Lett. **119**, 052401 (2021).
[11] A. Chanda, C. Holzmann, N. Schulz, J. Seyd, M. Albrecht, M. H. Phan, and H. Srikanth, Adv. Funct. Mater. **32**, 2109170 (2022).
[12] *Handbook of Magnetic Materials*, edited by E. P. Wohlfarth (Elsevier, North-Holland Amsterdam, 1980), Vol. 2.
[13] S. Ding, Z. Liang, C. Yun, R. Wu, M. Xue, Z. Lin, A. Ross, S. Becker, W. Yang, X. Ma, D. Chen, K. Sun, G. Jakob, M. Kläui, and J. Yang, Phys. Rev. B **104**, 224410 (2021).
[14] N. Nagaosa, J. Sinova, S. Onoda, A. H. MacDonald, and N. P. Ong, Rev. Mod. Phys. **82**, 1539 (2010).
[15] H. Nakayama, M. Althammer, Y. T. Chen, K. Uchida, Y. Kajiwara, D. Kikuchi, T. Ohtani, S. Geprags, M. Opel, S. Takahashi, R. Gross, G. E. Bauer, S. T. Goennenwein, and E. Saitoh, Phys. Rev. Lett. **110**, 206601 (2013).
[16] Y. Chen, S. Takahashi, H. Nakayama, M. Althammer, S. T. B. Goennenwein, E. Saitoh, and G. E. W. Bauer, Phys. Rev. B **87**, 144411 (2013).
[17] Y. F. Li, X. H. Yang, H. Bai, M. Z. Wang, D. S. Cheng, C. Song, Z. Yuan, Y. Liu, and Z. Shi, Phys. Rev. B **108**, 184403 (2023).
[18] T. Fu, S. Li, X. Feng, Y. Cui, J. Yao, B. Wang, J. Cao, Z. Shi, D. Xue, and X. Fan, Phys. Rev. B **103**, 064432 (2021).
[19] T. Xu, Y. Cheng, Y. Dong, H. Bai, H. Zhou, X. Shu, P. Gargiani, M. Valvidares, P. Yu, and W. Jiang, Phys. Rev. Appl. **19**, 034088 (2023).
[20] W. Zhang, M. B. Jungfleisch, W. Jiang, Y. Liu, J. E. Pearson, S. G. E. t. Velthuis, A. Hoffmann, F. Freimuth, and Y. Mokrousov, Phys. Rev. B **91**, 115316 (2015).
[21] L. Liu, J. Ye, H. Yang, L. Lin, and H. An, Appl. Phys. Lett. **124**, 132409 (2024).
[22] P. G. Li, J. M. Liang, S. M. Ng, H. F. Wong, Y. Zhou, L. J. Huang, K. W. Lin, Y. H. Tsang, C. L. Mak, and C. W. Leung, J. Magn. Magn. Mater. **592**, 171785 (2024).
[23] C. Tang, P. Sellappan, Y. Liu, Y. Xu, J. E. Garay, and J. Shi, Phys. Rev. B **94**, 140403 (2016).
[24] H. Fuess, G. Bassi, M. Bonnet, and A. Delapalme, Solid State Commun. **18**, 557 (1976).

[25]S. M. Zanjani and M. C. Onbaşlı, J. Magn. Magn. Mater. **499**, 166108 (2020).
[26]V. H. Ortiz, M. Aldosary, J. Li, Y. Xu, M. I. Lohmann, P. Sellappan, Y. Kodera, J. E. Garay, and J. Shi, APL Mater. **6**, 121113 (2018).
[27]V. H. Ortiz, B. Arkook, J. Li, M. Aldosary, M. Biggerstaff, W. Yuan, C. Warren, Y. Kodera, J. E. Garay, I. Barsukov, and J. Shi, Phys. Rev. Mater. **5**, 124414 (2021).
[28]S. M. Zanjani and M. C. Onbasli, AIP Adv. **9**, 035024 (2019).
[29]Y. K. Liu, J. M. Liang, H. F. Wong, S. M. Ng, C. L. Mak, and C. W. Leung, J. Magn. Magn. Mater. **536**, 168130 (2021).
[30]R. Yadav, A. Bake, W. T. Lee, Y. Liu, D. R. G. Mitchell, X. Yang, D. L. Cortie, K. Lin, and C. W. Leung, Phys. Rev. Mater. **7**, 124407 (2023).
[31]J. M. Gomez-Perez, S. Vélez, L. McKenzie-Sell, M. Amado, J. Herrero-Martín, J. López-López, S. Blanco-Canosa, L. E. Hueso, A. Chuvilin, J. W. A. Robinson, and F. Casanova, Phys. Rev. Appl. **10**, 044046 (2018).
[32]E. R. Rosenberg, L. Beran, C. O. Avci, C. Zeledon, B. Song, C. Gonzalez-Fuentes, J. Mendil, P. Gambardella, M. Veis, C. Garcia, G. S. D. Beach, and C. A. Ross, Phys. Rev. Mater. **2**, 094405 (2018).
[33]Y. Wang, X. Wang, A. T. Clark, H. Chen, X. M. Cheng, J. W. Freeland, and J. Q. Xiao, Phys. Rev. Mater. **5**, 074409 (2021).
[34]W. P. Wolf and J. H. Van Vleck, Phys. Rev. **118**, 1490 (1960).
[35]S. Becker, Z. Ren, F. Fuhrmann, A. Ross, S. Lord, S. Ding, R. Wu, J. Yang, J. Miao, M. Kläui, and G. Jakob, Phys. Rev. Appl. **16**, 014047 (2021).
[36]S. Damerio and C. O. Avci, J. Appl. Phys. **133**, 073902 (2023).
[37]Q. Shao, A. Grutter, Y. Liu, G. Yu, C. Yang, D. A. Gilbert, E. Arenholz, P. Shafer, X. Che, C. Tang, M. Aldosary, A. Navabi, Q. L. He, B. J. Kirby, J. Shi, and K. L. Wang, Phys. Rev. B **99**, 104401 (2019).
[38]X. Liang, Y. Zhu, B. Peng, L. Deng, J. Xie, H. Lu, M. Wu, and L. Bi, ACS Appl. Mater. Interfaces **8**, 8175 (2016).
[39]L. Jin, K. Jia, D. Zhang, B. Liu, H. Meng, X. Tang, Z. Zhong, and H. Zhang, ACS Appl. Mater. Interfaces **11**, 35458 (2019).
[40]J. J. Bauer, E. R. Rosenberg, and C. A. Ross, Appl. Phys. Lett. **114**, 052403 (2019).
[41]R. Kumar, S. N. Sarangi, D. Samal, and Z. Hossain, Phys. Rev. B **103**, 064421 (2021).
[42]J. M. Liang, X. W. Zhao, X. Yuan, Y. K. Liu, S. M. Ng, H. F. Wong, P. G. Li, Y. Zhou, F. X. Zhang, C. L. Mak, and C. W. Leung, Appl. Phys. Lett. **123**, 092405 (2023).
[43]S. M. Suturin, A. M. Korovin, V. E. Bursian, L. V. Lutsev, V. Bourobina, N. L. Yakovlev, M. Montecchi, L. Pasquali, V. Ukleev, A. Vorobiev, A. Devishvili, and N. S. Sokolov, Phys. Rev. Mater. **2**, 104404 (2018).